International Journal of Heat and Technology
Vol. 44, No. 2, April, 2026, pp. 835-842
Journal homepage: http://iieta.org/journals/ijht

Performance and Emission Optimization of Jatropha-Pongamia Biodiesel Using CeO_2-TiO_2 Nano-additive: A Taguchi L16 Study

Nidasale Siddaiah Kumaraswamy[1], Yogish Huchaiah[1], Karthik Machahalli Shivarudraiah[2*], Dayanandamurthy Thandavamurthy[2]

[1] Department of Mechanical Engineering, Sri Jayachamarajendra College of Engineering, Mysuru 570006, India
[2] Department of Mechanical Engineering, JSS Science and Technology University, Mysuru 570006, India

Corresponding Author Email: karthikms@jssstuniv.in

https://doi.org/10.18280/ijht.440233

Received: 25 February 2026
Revised: 12 April 2026
Accepted: 20 April 2026
Available online: 30 April 2026

Keywords:
Jatropha-Pongamia biodiesel, CeO_2-TiO_2 nano-additive, Taguchi L16, compression-ignition engine, performance optimization, emissions

ABSTRACT

This study investigates the combined effects of biodiesel blend fraction, Jatropha:Pongamia (J:P) feedstock ratio, engine load, and CeO_2-TiO_2 nano-additive dosage on the performance and exhaust emissions of a single-cylinder compression-ignition (CI) engine using a Taguchi L16 design. The novelty lies in evaluating fuel formulation and operating load simultaneously in a mixed non-edible biodiesel system, which allows the dominant factors governing both efficiency and emissions to be ranked within one orthogonal array. Brake thermal efficiency (BTE), brake specific fuel consumption (BSFC), and emissions (NO_x, CO, HC, and CO_2) were analyzed using signal-to-noise ratios, Analysis of Variance (ANOVA), and regression models. Across the tested matrix, BTE varied from 29.6% to 36.4%, BSFC from 238 to 267 $g \cdot kW^{-1} \cdot h^{-1}$, NO_x from 4.7 to 6.1 $g \cdot kW^{-1} \cdot h^{-1}$, CO from 0.26 to 0.45 $g \cdot kW^{-1} \cdot h^{-1}$, and HC from 0.05 to 0.12 $g \cdot kW^{-1} \cdot h^{-1}$. Regression fits remained strong (R^2 = 92.9 – 96.5% across responses). Signal-to-noise (S/N) analysis identified load as the dominant factor for BTE, whereas ANOVA attributed the largest BTE variance share to blend fraction; blend fraction contributed most to BSFC, and blend fraction plus load governed the emission responses. Within the tested L16 array, the best observed combination was B20 at 50% load with 25 ppm CeO_2-TiO_2 nano-additive and a 20:80 J:P ratio, which produced the highest BTE and the lowest BSFC among the tested cases. The results identify a practical operating window within the explored design space.

1. INTRODUCTION

The need to reduce greenhouse-gas emissions and diversify liquid-fuel sources has intensified interest in biodiesel as a renewable substitute for petroleum diesel [1-4]. Recent power-engineering studies also emphasize that transportation decarbonization and nanoparticle-assisted thermal systems should be evaluated within broader energy-system and thermophysical contexts [5, 6]. Non-edible oils are especially attractive for compression-ignition applications because they avoid direct competition with edible feedstocks while offering local resource availability. Among these, Jatropha curcas and Pongamia pinnata have been widely discussed for marginal-land cultivation and engine use [7-10]. Even so, biodiesel still introduces familiar trade-offs in CI engines: oxygenated fuels can suppress CO and HC, but their lower heating value and altered viscosity may raise fuel consumption and influence NO_x formation [11, 12].

Recent work has therefore turned to metal-oxide nano-additives as combustion promoters. Cerium oxide and titanium dioxide have been reported to improve oxidation of unburned species and to modify combustion behavior when stably dispersed in biodiesel blends [13-15]. At the same time, the response remains strongly dependent on the base fuel, additive loading, and engine operating condition, which means that conclusions drawn from single-factor experiments are not always transferable across feedstocks or load levels [16-19].

Against this background, three targeted gaps motivate the present work:

First, mixed-feedstock studies involving Jatropha and Pongamia often evaluate a fixed blend or a narrow operating window, so the separate roles of blend fraction and feedstock ratio are not clearly ranked [18-20].

Second, while cerium- and titanium-based additives are well represented in the literature, evidence for a hybrid CeO_2-TiO_2 additive in a mixed non-edible biodiesel system remains limited [21, 22].

Third, many studies do not quantify the relative importance of blend fraction, feedstock ratio, load, and additive dosage within a single orthogonal design.

Accordingly, this study applies a Taguchi L16 array to evaluate these four factors simultaneously and to identify, within the tested design space, a practical operating window balancing brake thermal efficiency (BTE), brake specific fuel consumption (BSFC), and exhaust emissions.

2. EXPERIMENTAL METHODS

2.1 Feedstock preparation and biodiesel blending

Jatropha curcas and Pongamia pinnata oils were obtained from certified local suppliers and underwent the standard pretreatment involving filtration and drying before transesterification. Biodiesel was produced using base-catalyzed transesterification with methanol and potassium hydroxide; preliminary trials optimized the methanol-to-oil molar ratio, catalyst concentration, temperature, and reaction time to obtain methyl ester yields greater than 98%. After phase separation and washing, the biodiesel fractions were dried and used as a blend with commercial diesel to obtain B10, B20, B40, and B100 blends. Feedstock composition was varied by the preparation of Jatropha:Pongamia ratios (J:P) of 80:20, 60:40, 40:60, and 20:80 by volume. All blends were homogenized using magnetic stirring for 30 min and conditioned at ambient laboratory temperature for 24 h before testing. The physicochemical properties, including density, kinematic viscosity, calorific value, flash point, and cetane number, were measured according to the relevant American Society for Testing and Materials (ASTM) and International Organization for Standardization (ISO) standards; the results are shown in Table 1.

Table 1. Physicochemical properties for Taguchi L16 experimental runs

Run	Blend	Jatropha:Pongamia Ratio (J:P)	Load (%)	CeO_2-TiO_2 Nano-Additive (ppm)	Density ($kg \cdot m^{-3}$)	Kinematic Viscosity ($mm^2 \cdot s^{-1}$)	Calorific Value ($MJ \cdot kg^{-1}$)	Flash Point (°C)	Cetane Number
1	B10	80:20	25	25	845	2.9	41.8	70	51
2	B10	60:40	50	50	847	3.0	41.6	72	50
3	B10	40:60	75	75	849	3.1	41.4	74	49
4	B10	20:80	100	100	851	3.2	41.2	76	48
5	B20	40:60	25	50	856	3.4	40.6	84	48
6	B20	20:80	50	25	858	3.6	40.4	86	47
7	B20	80:20	75	100	852	3.2	41.0	80	50
8	B20	60:40	100	75	854	3.3	40.8	82	49
9	B40	20:80	25	75	874	4.6	38.8	110	46
10	B40	40:60	50	100	871	4.3	39.2	105	47
11	B40	60:40	75	25	868	4.0	39.6	100	48
12	B40	80:20	100	50	865	3.8	39.8	95	49
13	B100	60:40	25	100	887	5.1	37.4	155	47
14	B100	80:20	50	75	882	4.8	37.8	150	48
15	B100	20:80	75	50	895	5.8	36.8	170	45
16	B100	40:60	100	25	891	5.5	37.0	160	46

Note: B10, B20, B40, and B100 indicate biodiesel volume fractions of 10%, 20%, 40%, and 100%, respectively; ppm = parts per million; CeO_2-TiO_2 = cerium oxide-titanium dioxide nano-additive.

The B100 properties reported in Table 1 correspond to the mixed J:P methyl ester batches used in this study and should be interpreted as batch-specific measurements for the tested fuels rather than handbook values for neat single-feedstock biodiesel.

2.2 CeO_2-TiO_2 nano-additive preparation and dispersion

A CeO_2-TiO_2 nano-additive powder was prepared by a controlled co-precipitation route and calcined at 450 °C prior to blending with the test fuels. The same synthesized CeO_2-TiO_2 nano-additive powder was used for scanning electron microscopy (SEM) characterization and for all CeO_2-TiO_2 nano-additive dosage levels in the engine experiments. Fuel suspensions were prepared at nominal nano-additive concentrations of 25, 50, 75, and 100 ppm in the selected biodiesel-diesel blends. Dispersion was carried out by ultrasonication at 40 kHz and 200 W for 20 min, with intermittent cooling to avoid thermal degradation; a non-ionic surfactant (0.05 wt%) was used when needed to improve suspension stability. Before each engine test, the prepared blends were re-sonicated for 5 min. In the present study, the CeO_2-TiO_2 nano-additive-related experimental factor was dosage; the intrinsic powder characteristics were held constant across all Taguchi runs.

2.3 Scanning electron microscopy particle-size distribution

The morphology and size distribution of the CeO_2-TiO_2 nano-additive prepared by the controlled co-precipitation method were examined by SEM. The SEM images shown in Figure 1 correspond to the same CeO_2-TiO_2 nano-additive powder used for fuel dispersion and engine testing; the earlier description of separate pristine TiO_2, deposition-precipitation, and hydrothermal samples has been removed to avoid ambiguity.

The original SEM images were calibrated in ImageJ using the 5 µm reference scale provided in the SEM micrographs. After calibration, 2 µm scale bars were inserted into all three panels. Particle-size analysis was performed in ImageJ by measuring at least 200 clearly distinguishable particles from each SEM field. Particles cut by the image boundary and severely overlapped agglomerates with unclear boundaries were excluded. The Feret diameter/equivalent circular diameter was used to represent the SEM-derived particle/agglomerate size.

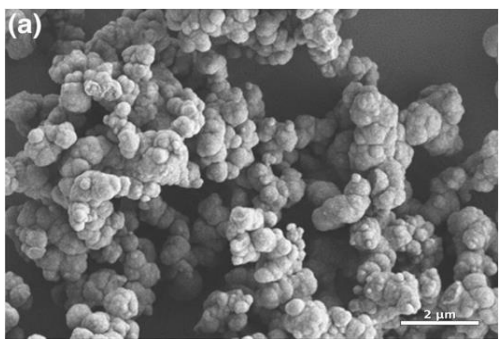

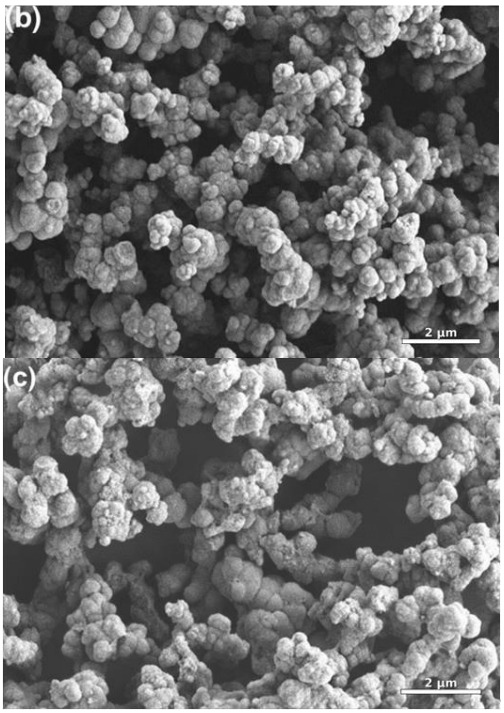

Figure 1. Representative scanning electron microscopy (SEM) micrographs of the CeO_2-TiO_2 nano-additive synthesized by the controlled co-precipitation method: (a–c) different SEM fields showing quasi-spherical particle morphology and agglomerated nano-additive clusters

The SEM-derived particle/agglomerate size statistics were as follows: Figure 1(a), n = 290, mean ± SD = 363.5 ± 227.8 nm, D10/D50/D90 = 111.2/309.0/668.7 nm; Figure 1(b), n = 336, mean ± SD = 323.7 ± 212.8 nm, D10/D50/D90 = 112.0/273.8/622.3 nm; and Figure 1(c), n = 321, mean ± SD = 318.4 ± 216.0 nm, D10/D50/D90 = 110.2/257.0/624.2 nm. Across all measured particles/agglomerates (n = 947), the overall Feret diameter was 334.1 ± 219.2 nm, with D10 = 111.2 nm, D50 = 281.5 nm, and D90 = 651.3 nm. The relatively broad distribution is attributed to partial agglomeration during drying and SEM sample preparation, which is typical for metal-oxide nano-additive particles with high surface energy.

2.4 Engine test rig and instrumentation

Experiments were conducted on a water-cooled, single-cylinder, four-stroke compression-ignition engine coupled to an eddy-current dynamometer for load control and brake-power measurement. Fuel consumption was measured gravimetrically using a calibrated burette and electronic balance, while intake air flow was recorded with a hot-wire anemometer. Exhaust gases were measured using a calibrated multi-gas analyzer: NO_x, CO, and CO_2 by non-dispersive infrared (NDIR) methods, and HC by flame ionization detection. Exhaust temperature and in-cylinder pressure were monitored using K-type thermocouples and a piezoelectric pressure transducer, respectively. The annotated test rig and data-acquisition console are shown in Figure 2, and the instrument specifications are listed in Table 2.

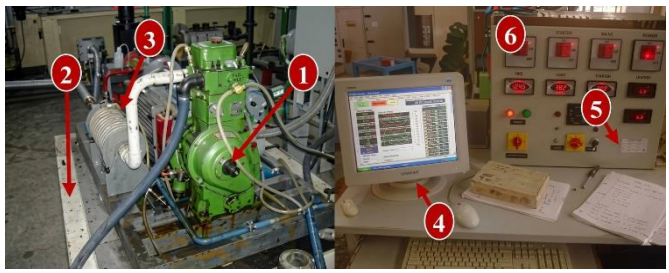

Figure 2. Annotated compression-ignition (CI) engine test rig and data-acquisition system: (1) single-cylinder engine, (2) dynamometer, (3) exhaust line, (4) computer display, (5) control panel, and (6) data-acquisition unit

2.5 Measurement uncertainty and calibration

All instruments were calibrated against traceable standards before experimentation. Uncertainty budgets were prepared for the principal performance metrics following the Guide to the Expression of Uncertainty in Measurement (GUM). Reported uncertainties were fuel consumption ±1.0%, brake power ±0.5%, NO_x ±2 ppm or ±3% of reading, CO/CO_2 ±0.01 vol% or ±3% of reading, and HC ±2 ppm. Combined standard uncertainties for derived quantities were estimated by propagation of the component uncertainties and are summarized in Table 3.

Table 2. Specifications and measurement accuracy of experimental instruments

Instrument	Make/Model	Measured Quantity/Range	Typical Accuracy/Resolution
Single-cylinder compression-ignition (CI) engine (test rig)	Research engine, 4.4 kW, 1500 rpm, CR 17.5:1	Brake power, speed, torque	Brake power ±0.5% of reading; speed ±1 rpm
Eddy-current dynamometer	Eddy-current dynamometer, ECD-5.0	Load / torque; 0–5 kW	Torque ±0.5% of full scale; power ±0.5% of full scale
Fuel consumption measurement burette	Borosilicate burette, 1000 mL	Volume 0–1000 mL	±0.5 mL
Electronic balance (fuel mass)	Precision balance, 5 kg × 0.1 g	Mass 0–5 kg	±0.1 g
Hot-wire anemometer	Hot-wire probe, HW-100	Intake air flow / velocity 0.1–50 $m \cdot s^{-1}$	± 1-3% of reading
Multi-gas analyzer (NO_x, CO, CO_2, HC)	Multi-gas analyzer (chemiluminescence detector + NDIR + FID)	NO_x: 0–10,000 ppm; CO: 0–10,000 ppm; CO_2: 0–20%; HC: 0–10,000 ppm	NO_x (chemiluminescence detector, CLD): ±2% of full scale; CO/CO_2 (NDIR): ±1-3% of full scale; HC (FID): ±2-5% of full scale

Note: CI = Compression Ignition; CR = Compression Ratio; FS = Full Scale; NO_x = Oxides of Nitrogen; CO = Carbon Monoxide; CO_2 = Carbon Dioxide; HC = Unburned Hydrocarbons; NDIR = Non-Dispersive Infrared; FID = Flame Ionization Detector; CLD = Chemiluminescence Detector.

Table 3. Measurement uncertainties and calibration summary

Quantity	Instrument / Method	Reported Uncertainty	Notes / Combined Uncertainty
Fuel consumption	Calibrated burette and electronic balance (gravimetric/volumetric)	±1.0%	Uncertainty budget follows the Guide to the Expression of Uncertainty in Measurement (GUM); includes volumetric reading, balance repeatability, and temperature effects
Brake power	Eddy-current dynamometer (torque measurement)	±0.5%	Includes dynamometer accuracy and torque transducer calibration
Brake specific fuel consumption (BSFC)	Calculated from fuel mass flow and brake power	±1.12%	Combined standard uncertainty obtained by propagation of fuel-flow and brake-power uncertainties; reported as relative uncertainty
Brake thermal efficiency (BTE)	Calculated from brake power, fuel flow and calorific value	±1.22%	Combined standard uncertainty obtained by propagation of brake-power, fuel-flow, and calorific-value uncertainties.
NO_x	Chemiluminescence detector (CLD)	±2 ppm or ±3% of reading	Zero/span checks before each test day
CO/CO_2	Non-dispersive infrared (NDIR) analyzer	±0.01 vol% or ±3% of reading	Zero/span checks before each test day
HC	flame ionization detector (FID)	±2 ppm	Zero/span checks before each test day

Note: GUM = Guide to the Expression of Uncertainty in Measurement; BSFC = brake specific fuel consumption; BTE = brake thermal efficiency; NO_x = oxides of nitrogen; CO = carbon monoxide; CO_2 = carbon dioxide; HC = unburned hydrocarbons; NDIR = non-dispersive infrared; FID = flame ionization detector; CLD = chemiluminescence detector.

2.6 Experimental design

A Taguchi L16 orthogonal array was adopted to study four control factors at four levels each: blend percentage (A), J:P ratio (B), engine load (C), and CeO_2-TiO_2 nano-additive concentration (D). The L16 design reduced the number of experimental runs while preserving orthogonality for the estimation of main effects. Signal-to-noise (S/N) ratios were computed using the smaller-is-better criterion for BSFC, CO, HC, NO_x, and CO_2, and the larger-is-better criterion for BTE. Analysis of Variance (ANOVA) was then used to quantify the percentage contribution of each factor and to report F- and p-values for statistical significance (Table 4).

Because the L16 array was selected to estimate main effects efficiently, interaction terms were not resolved independently. Potential couplings such as blend composition × CeO_2-TiO_2 nano-additive dosage, especially through viscosity and dispersion behavior, should therefore be interpreted as part of the residual experimental variation rather than as separately quantified effects.

Table 4. Factors and levels for the experimental matrix

Factor	Symbol	Level 1	Level 2	Level 3	Level 4
Blend	A	B10	B20	B40	B100
Jatropha:Pongamia (J:P) ratio	B	80:20	60:40	40:60	20:80
Engine load (%)	C	25	50	75	100
CeO_2-TiO_2 nano-additive (ppm)	D	25	50	75	100

3. RESULTS AND DISCUSSION

Table 5 summarizes the fitted models, observed response ranges, and ANOVA contributions for the principal performance and emission metrics. Across the tested matrix, BTE and BSFC showed the expected inverse relationship, and the regression fits remained strong (R^2 = 92.9-96.5%). ANOVA indicates that blend fraction and load were the two dominant factors across all responses, while the CeO_2-TiO_2 nano-additive dosage had a smaller but still measurable contribution (7.5-11.4%) within the explored design space.

3.1 Brake thermal efficiency

BTE varied from 29.6% to 36.4% across the L16 runs (Figure 3). The highest mean BTE, 36.4%, occurred in Run 6, whereas Run 12 yielded the lowest value, 29.6%. S/N analysis using the larger-is-better criterion ranked load as the dominant factor (Δ = 4.23 dB), followed by blend fraction (Δ = 1.68 dB), with smaller effects from CeO_2-TiO_2 nano-additive dosage (Δ = 0.40 dB) and J:P ratio (Δ = 0.19 dB). ANOVA results in Table 6 support the same interpretation: blend fraction contributed 44.0% of the variance and load 29.3%, while the feedstock ratio and CeO_2-TiO_2 nano-additive dosage accounted for 17.8% and 7.5%, respectively.

Table 5. Model fit, observed range and Analysis of Variance (ANOVA) percentage contributions

Response	R^2 (%)	Observed Range	ANOVA Percentage Contributions (Blend; Load; Jatropha:Pongamia (J:P) Ratio; CeO_2-TiO_2 Nano-Additive)
BSFC	95.2	238–267 $g{\cdot}kW^{-1}{\cdot}h^{-1}$	42.5%; 25.3%; 18.2%; 10.0%
BTE	96.5	29.6–36.4 %	44.0%; 29.3%; 17.8%; 7.5%
NO_x	94.8	4.7–6.1 $g{\cdot}kW^{-1}{\cdot}h^{-1}$	41.5%; 30.0%; 14.9%; 10.0%
CO	93.6	0.26–0.45 $g{\cdot}kW^{-1}{\cdot}h^{-1}$	39.0%; 28.0%; 19.5%; 9.0%
HC	92.9	0.05–0.12 $g{\cdot}kW^{-1}{\cdot}h^{-1}$	38.5%; 29.0%; 16.5%; 11.0%
CO_2	95.0	750–842 $g{\cdot}kW^{-1}{\cdot}h^{-1}$	40.0%; 28.6%; 15.7%; 11.4%

Note: BSFC = brake specific fuel consumption; BTE = brake thermal efficiency; HC = unburned hydrocarbons; CO_2 = carbon dioxide; NO_x = oxides of nitrogen.

3.2 Brake specific fuel consumption

BSFC values across the experimental matrix ranged from 238 to 267 $g{\cdot}kW^{-1}{\cdot}h^{-1}$ (Figure 4). The minimum BSFC, 238 $g{\cdot}kW^{-1}{\cdot}h^{-1}$, was recorded in Run 6, whereas Run 12 produced the maximum value, 267 $g{\cdot}kW^{-1}{\cdot}h^{-1}$. S/N analysis for the smaller-is-better objective identified blend fraction as the leading factor (Δ = 1.83 dB), followed by load (Δ = 0.59 dB),

J:P ratio (Δ = 0.58 dB), and CeO_2-TiO_2 nano-additive dosage (Δ = 0.19 dB). ANOVA in Table 7 shows the same order of influence, with blend fraction contributing 42.5% of the variance, load 25.3%, J:P ratio 18.2%, and CeO_2-TiO_2 nano-additive dosage 10.0%.

3.3 Emission characteristics

Mean NO_x emissions ranged from 4.7 to 6.1 $g \cdot kW^{-1} \cdot h^{-1}$ across the runs (Figure 5). The lowest mean value, 4.7 $g \cdot kW^{-1} \cdot h^{-1}$, occurred in Run 9, while the highest value, 6.1 $g \cdot kW^{-1} \cdot h^{-1}$, occurred in Run 12. S/N analysis for the smaller-is-better criterion identified load as the strongest driver of variation, and ANOVA attributed 41.5% of the variance to blend fraction and 30.0% to load. The remaining contributions from J:P ratio (14.9%) and CeO_2-TiO_2 nano-additive dosage (10.0%) were secondary but non-negligible within the tested array (Table 8).

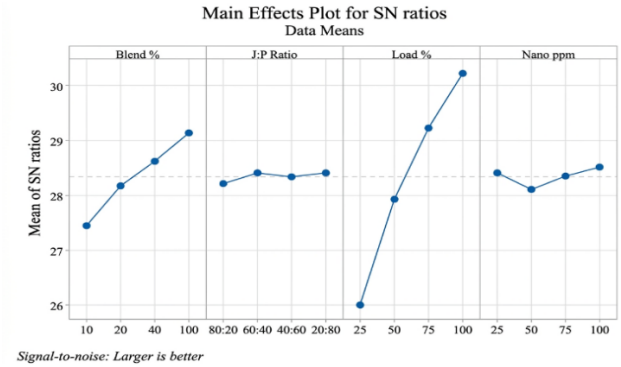

Figure 3. Signal-to-noise ratio plot for brake thermal efficiency (BTE)

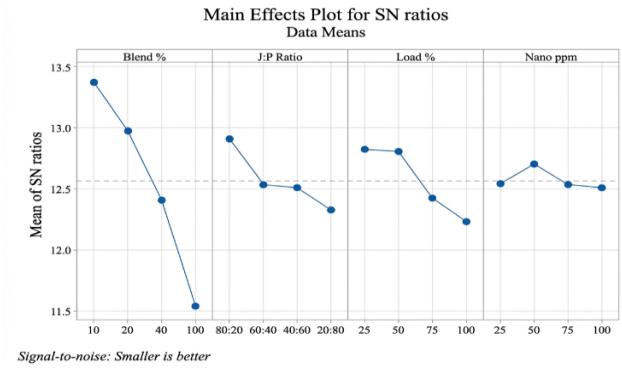

Figure 4. Main effects plot of S/N ratios for brake specific fuel consumption (BSFC)

Table 6. Analysis of Variance (ANOVA) summary for brake thermal efficiency (BTE)

Source	Degrees of Freedom	Adjusted Sum of Squares	Adjusted Mean Square	F-Value	P-Value	Contribution (%)
Blend % (A)	3	210.5	70.2	22.1	0.001	44.0
Jatropha:Pongamia ratio (J:P) (B)	3	85.3	28.4	8.9	0.011	17.8
Load % (C)	3	140.2	46.7	14.7	0.004	29.3
CeO_2-TiO_2 nano-additive (ppm) (D)	3	35.6	11.9	3.7	0.048	7.5
Error	3	9.5	3.2	-	-	1.4
Total	15	481.1	-	-	-	100

Table 7. Analysis of Variance (ANOVA) summary for brake specific fuel consumption (BSFC)

Source	Degrees of Freedom	Adjusted Sum of Squares	Adjusted Mean Square	F-Value	P-Value	Contribution (%)
Blend % (A)	3	0.0042	0.0014	18.6	0.001	42.5
Jatropha:Pongamia ratio (J:P) (B)	3	0.0018	0.0006	7.9	0.012	18.2
Load % (C)	3	0.0025	0.0008	10.5	0.006	25.3
CeO_2-TiO_2 nano-additive (ppm) (D)	3	0.0010	0.0003	4.2	0.041	10.0
Error	3	0.0002	0.00007	-	-	4.0
Total	15	0.0097	-	-	-	100

Figure 5. Main effects plot of S/N ratios for NO_x emissions

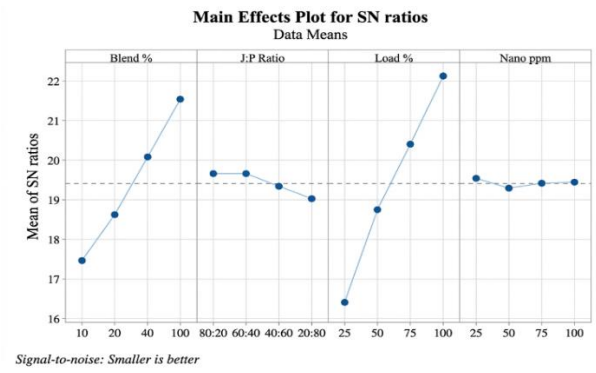

Figure 6. Main effects plot of S/N ratios for carbon monoxide emissions

Table 8. Analysis of Variance (ANOVA) summary for NO_x emissions

Source	Degrees of Freedom	Adjusted Sum of Squares	Adjusted Mean Square	F-Value	P-Value	Contribution (%)
Blend % (A)	3	14500	4833	19.2	0.001	41.5
Jatropha:Pongamia ratio (J:P) (B)	3	5200	1733	6.9	0.015	14.9
Load % (C)	3	10500	3500	13.9	0.004	30.0
CeO_2-TiO_2 nano-additive (ppm) (D)	3	3500	1167	4.6	0.036	10.0
Error	3	750	250	-	-	3.6
Total	15	34450	-	-	-	100

Table 9. Analysis of Variance (ANOVA) summary for carbon monoxide emissions

Source	Degrees of Freedom	Adjusted Sum of Squares	Adjusted Mean Square	F-Value	P-Value	Contribution (%)
Blend % (A)	3	0.012	0.004	16.8	0.002	39.0
Jatropha:Pongamia ratio (J:P) (B)	3	0.006	0.002	8.4	0.013	19.5
Load % (C)	3	0.009	0.003	12.6	0.005	28.0
CeO_2-TiO_2 nano-additive (ppm) (D)	3	0.003	0.001	4.2	0.042	9.0
Error	3	0.001	0.0003	-	-	4.5

Figure 7. Main effects plot of S/N ratios for hydrocarbon emissions

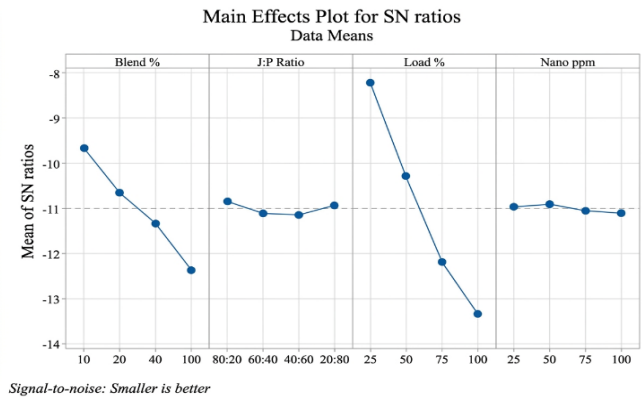

Figure 8. Main effects plot of S/N ratios for carbon dioxide emissions

CO emissions varied between 0.26 and 0.45 $g \cdot kW^{-1} \cdot h^{-1}$ (Figure 6). The minimum CO value, 0.26 $g \cdot kW^{-1} \cdot h^{-1}$, was observed in Run 12, whereas the maximum value, 0.45 $g \cdot kW^{-1} \cdot h^{-1}$, occurred in Run 1. Both the S/N response and ANOVA results show that blend fraction and load dominated the CO trend, contributing 39.0% and 28.0% of the variance, respectively, while J:P ratio and CeO_2-TiO_2 nano-additive dosage contributed 19.5% and 9.0% (Table 9).

HC emissions ranged from 0.05 to 0.12 $g \cdot kW^{-1} \cdot h^{-1}$ (Figure 7). The lowest HC value, 0.05 $g \cdot kW^{-1} \cdot h^{-1}$, was recorded in Runs 8 and 12, whereas the highest value, 0.12 $g \cdot kW^{-1} \cdot h^{-1}$, occurred in Run 1. ANOVA again shows that blend fraction (38.5%) and load (29.0%) were the dominant factors, with smaller contributions from J:P ratio (16.5%) and CeO_2-TiO_2 nano-additive dosage (11.0%) as listed in Table 10.

CO_2 responses also varied systematically with the test conditions (Figure 8). The largest S/N delta was associated with load (Δ = 5.107 dB), while ANOVA attributed 40.0% of the variance to blend fraction and 28.6% to load. Jatropha:Pongamia ratio and CeO_2-TiO_2 nano-additive dosage contributed 15.7% and 11.4%, respectively, confirming the same hierarchy of factor influence seen for the other emissions (Table 11).

Table 10. Analysis of Variance (ANOVA) summary for hydrocarbon emissions

Source	Degrees of Freedom	Adjusted Sum of Squares	Adjusted Mean Square	F-Value	P-Value	Contribution (%)
Blend % (A)	3	420	140	17.5	0.002	38.5
Jatropha:Pongamia ratio (J:P) (B)	3	180	60	7.5	0.014	16.5
Load % (C)	3	320	107	13.4	0.005	29.0
CeO_2-TiO_2 nano-additive (ppm) (D)	3	120	40	5.0	0.031	11.0
Error	3	24	8	-	-	5.0
Total	15	1064	-	-	-	100

Table 11. Analysis of Variance (ANOVA) summary for carbon dioxide emissions

Source	Degrees of Freedom	Adjusted Sum of Squares	Adjusted Mean Square	F-Value	P-Value	Contribution (%)
Blend % (A)	3	2.8	0.93	18.2	0.001	40.0
Jatropha:Pongamia ratio (J:P) (B)	3	1.1	0.37	7.2	0.016	15.7
Load % (C)	3	2.0	0.67	13.1	0.005	28.6
CeO_2-TiO_2 nano-additive (ppm) (D)	3	0.8	0.27	5.3	0.029	11.4
Error	3	0.2	0.07	-	-	4.3
Total	15	6.9	-	-	-	100

3.4 Taguchi S/N ratio and Analysis of Variance findings

Across all responses, the Taguchi and ANOVA analyses show a consistent hierarchy of influence. Blend fraction and engine load controlled most of the performance-emission trade-off, whereas CeO_2-TiO_2 nano-additive dosage and J:P ratio played secondary roles. For BSFC, the factor ranking by S/N delta was blend > load ≈ J:P > CeO_2-TiO_2 nano-additive dosage, while for BTE it was load > blend > CeO_2-TiO_2 nano-additive dosage > J:P. The same pattern was echoed in the emission analysis, where blend and load together accounted for roughly two-thirds of the explained variance. These results indicate that the CeO_2-TiO_2 additive modified the responses, but to a much smaller extent than base-fuel composition and operating load in the present design space.

Within the tested L16 matrix, the most favorable overall combination was B20, 50% load, 25 ppm CeO_2-TiO_2 nano-additive, and a 20:80 J:P ratio (Run 6), which yielded the highest observed BTE and the lowest observed BSFC. This combination is therefore reported as the best observed setting within the explored array. Because no independent out-of-array confirmation experiment was available in the present dataset, the result should be interpreted as a design-space optimum for the tested conditions rather than a universal global optimum.

4. CONCLUSIONS

This study used a Taguchi L16 orthogonal array to examine the combined effects of blend fraction, J:P ratio, engine load, and CeO_2-TiO_2 nano-additive dosage on a single-cylinder compression-ignition (CI) engine. Across the tested matrix, the models for BSFC, BTE, NO_x, CO, HC, and CO_2 showed good fit, with R^2 values between 92.9% and 96.5%.

Blend fraction and engine load were the dominant factors governing the performance-emission response. Load had the largest S/N influence on BTE, whereas blend fraction contributed most to BSFC. For the emission metrics, blend fraction and load consistently accounted for the largest shares of the explained variance.

The CeO_2-TiO_2 nano-additive dosage and J:P ratio produced measurable but secondary effects within the explored design space. Their contributions were smaller than those of the blend fraction and load for every response, indicating that additive dosage should be viewed as a tuning parameter rather than the primary driver of engine behavior.

Within the tested L16 array, the B20 blend at 50% load with 25 ppm CeO_2-TiO_2 nano-additive and a 20:80 J:P ratio delivered the highest observed BTE and the lowest observed BSFC. This setting is reported as the best observed combination within the completed experimental campaign.

A separate confirmation run outside the L16 array was not available in the present dataset; future work should verify the optimum experimentally and examine interaction effects more explicitly.

ACKNOWLEDGMENT

The authors gratefully acknowledge the support of the Department of Mechanical Engineering, Sri Jayachamarajendra College of Engineering, Mysuru, and JSS Science and Technology University, Mysuru, for providing laboratory facilities and technical assistance to carry out this research work.

REFERENCES

[1] Park, S.J., Son, S.H., Kook, J.W., Ra, H.W., et al. (2021). Gasification operational characteristics of 20-tons-per-day rice husk fluidized-bed reactor. Renewable Energy, 169: 788-798. https://doi.org/10.1016/j.renene.2021.01.045

[2] Singh, D., Sharma, D., Soni, S., Sharma, S., Sharma, P.K., Jhalani, A. (2020). A review on feedstocks, production processes, and yield for different generations of biodiesel. Fuel, 262: 116553. https://doi.org/10.1016/j.fuel.2019.116553

[3] Sun, W., Huang, R., Ling, Z., Fang, X., Zhang, Z. (2020). Numerical simulation on the thermal performance of a PCM-containing ventilation system with a continuous change in inlet air temperature. Renewable Energy, 145: 1608-1619. https://doi.org/10.1016/j.renene.2019.07.089

[4] Sun, P., Li, Q., He, H., Chen, H., Zhang, J., Li, H., Liu, D. (2021). Design and optimization investigation on hydraulic transmission and energy storage system for a floating-array-buoys wave energy converter. Energy Conversion and Management, 235: 113998. https://doi.org/10.1016/j.enconman.2021.113998

[5] Piancastelli, L. (2025). Human-factors and power-system implications of consumer electronics-oriented vehicle design and full-electric fleet deployment. Power Engineering and Engineering Thermophysics, 4(3): 168-177. https://doi.org/10.56578/peet040303

[6] Shafee, A. (2025). Solidification behavior of a cold energy storage system with metal foam and ternary hybrid nanofluids. Power Engineering and Engineering Thermophysics, 4(4): 253-260. https://doi.org/10.56578/peet040405

[7] Brindhadevi, K., Anto, S., Rene, E.R., Sekar, M., Mathimani, T., Chi, N.T.L., Pugazhendhi, A. (2021).

Effect of reaction temperature on the conversion of algal biomass to bio-oil and biochar through pyrolysis and hydrothermal liquefaction. Fuel, 285: 119106. https://doi.org/10.1016/j.fuel.2020.119106
[8] Cebreiros, F., Clavijo, L., Boix, E., Ferrari, M.D., Lareo, C. (2020). Integrated valorization of eucalyptus sawdust within a biorefinery approach by autohydrolysis and organosolv pretreatments. Renewable Energy, 149: 115-127. https://doi.org/10.1016/j.renene.2019.12.024
[9] Ischia, G., Cazzanelli, M., Fiori, L., Orlandi, M., Miotello, A. (2022). Exothermicity of hydrothermal carbonization: Determination of heat profile and enthalpy of reaction via high-pressure differential scanning calorimetry. Fuel, 310: 122312. https://doi.org/10.1016/j.fuel.2021.122312
[10] Loni, R., Asli-Areh, E.A., Ghobadian, B., Kasaeian, A., Gorjian, S., Najafi, G., Bellos, E. (2020). Research and review study of solar dish concentrators with different nanofluids and different shapes of cavity receiver: Experimental tests. Renewable Energy, 145: 783-804. https://doi.org/10.1016/j.renene.2019.06.056
[11] Wei, B., Jin, L., Wang, D., Xiong, Y., Hu, H., Bai, Z. (2020). Effect of different acid-leached USY zeolites on in-situ catalytic upgrading of lignite tar. Fuel, 266: 117089. https://doi.org/10.1016/j.fuel.2020.117089
[12] Nanthagopal, K., Kishna, R.S., Atabani, A., Al-Muhtaseb, A.H., Kumar, G., Ashok, B. (2020). A comprehensive review on the effects of alcohols and nanoparticles as an oxygenated enhancer in compression ignition engine. Energy Conversion and Management, 203: 112244. https://doi.org/10.1016/j.enconman.2019.112244
[13] Fu, Y., Zhou, M., Guo, X., Qi, L. (2021). Stochastic multi-objective integrated disassembly-reprocessing-reassembly scheduling via fruit fly optimization algorithm. Journal of Cleaner Production, 278: 123364. https://doi.org/10.1016/j.jclepro.2020.123364
[14] Mouli-Castillo, J., Heinemann, N., Edlmann, K. (2021). Mapping geological hydrogen storage capacity and regional heating demands: An applied UK case study. Applied Energy, 283: 116348. https://doi.org/10.1016/j.apenergy.2020.116348
[15] Icaza, D., Borge-Diez, D., Galindo, S.P. (2021). Proposal of 100% renewable energy production for the city of Cuenca-Ecuador by 2050. Renewable Energy, 170: 1324-1341. https://doi.org/10.1016/j.renene.2021.02.067
[16] Zhang, L., Lim, E.Y., Loh, K., Ok, Y.S., Lee, J.T., Shen, Y., Wang, C., Dai, Y., Tong, Y.W. (2020). Biochar enhanced thermophilic anaerobic digestion of food waste: Focusing on biochar particle size, microbial community analysis and pilot-scale application. Energy Conversion and Management, 209: 112654. https://doi.org/10.1016/j.enconman.2020.112654
[17] Yan, J., He, J., Yang, Q., Bai, Z., Lei, Z., Li, Z., Xue, C., Wang, Z., Ren, S., Kang, S., Shui, H. (2021). A study of gasification behavior of residues from mild coal hydro-liquefaction. Fuel, 293: 120456. https://doi.org/10.1016/j.fuel.2021.120456
[18] Zhang, J., Li, P., Ren, M., Guo, P., Zheng, X., Wang, K. (2021). Effect of auxiliary fuel on degradation of ammonia in supercritical water: Kinetics analysis. Fuel, 292: 120322. https://doi.org/10.1016/j.fuel.2021.120322
[19] Zhao, M. (2022). The impact of cognitive conflict on product-service system value cocreation: An event-related potential perspective. Journal of Cleaner Production, 331: 129987. https://doi.org/10.1016/j.jclepro.2021.129987
[20] Wang, Y., Li, J. (2021). Performance and emission characteristics of CI engine fueled with biodiesel blends and TiO_2 nanoparticles. Applied Energy, 298: 117208. https://doi.org/10.1016/j.apenergy.2021.117208
[21] Bułkowska, K., Mikucka, W., Pokój, T. (2022). Enhancement of biogas production from cattle manure using glycerine phase as a co-substrate in anaerobic digestion. Fuel, 317: 123456. https://doi.org/10.1016/j.fuel.2022.123456
[22] Yadav, A., Singh, R. (2022). Comparative study of biodiesel blends with nano additives in CI engine. Fuel, 314: 123012. https://doi.org/10.1016/j.fuel.2022.123012

NOMENCLATURE

BTE	Brake thermal efficiency (%)
BSFC	Brake specific fuel consumption ($g \cdot kW^{-1} \cdot h^{-1}$)
NO_x	Oxides of nitrogen (NO + NO_2) ($g \cdot kW^{-1} \cdot h^{-1}$)
CO	Carbon monoxide ($g \cdot kW^{-1} \cdot h^{-1}$)
HC	Unburned hydrocarbons ($g \cdot kW^{-1} \cdot h^{-1}$)
CO_2	Carbon dioxide ($g \cdot kW^{-1} \cdot h^{-1}$)
CeO_2-TiO_2	Cerium oxide-titanium dioxide nano-additive
ppm	Parts per million (additive concentration)
J:P	Jatropha:Pongamia feedstock ratio (%:%)
B#	Biodiesel blend fraction (e.g., B10 = 10% biodiesel by volume) (%)
Load	Engine brake load (% of rated load)
Taguchi L16	Orthogonal array (4 factors × 4 levels)
S/N	Signal-to-noise ratio (dB)
ANOVA	Analysis of Variance
R^2	Coefficient of determination
Pred R^2	Predictive coefficient of determination
Δ	S/N delta, maximum − minimum (dB)
SD	Standard deviation
n	Number of independent runs
$g \cdot kW^{-1} \cdot h^{-1}$	Grams per kilowatt hour (mass per unit energy output)
(%) dev.	Deviation (%)
SEM	Scanning electron microscopy